Monosynaptic tracing maps brain-wide afferent oligodendrocyte precursor cell connectivity

Christopher W Mount*[,1,2,3], Belgin Yalçın*[,1], Kennedy Cunliffe-Koehler[1], Michelle Monje[1,4,5,6]

* These authors contributed equally to this work

1 Department of Neurology, Stanford University, Stanford CA
2 Medical Scientist Training Program, Stanford University, Stanford CA
3 Neurosciences Graduate Program, Stanford University, Stanford CA
4 Institute for Stem Cell Biology and Regenerative Medicine, Stanford University, Stanford CA
5 Department of Pathology, Stanford University, Stanford CA
6 Department of Pediatrics, Stanford University, Stanford CA

Abstract

Neurons form bona fide synapses with oligodendrocyte precursor cells (OPCs), but the circuit context of these neuron to OPC synapses remains incompletely understood. Using monosynaptically-restricted rabies virus tracing of OPC afferents, we identified extensive afferent synaptic inputs to OPCs residing in secondary motor cortex, corpus callosum, and primary somatosensory cortex of adult mice. These inputs primarily arise from functionally-interconnecting cortical areas and thalamic nuclei, demonstrating that OPCs have strikingly comprehensive synaptic access to brain-wide functionally-related projection networks. Quantification of these inputs revealed excitatory and inhibitory components that are consistent in number across brain regions and stable in barrel cortex despite whisker trimming-induced sensory deprivation.

Introduction

Excitatory and inhibitory synapses between neurons and OPCs are well-established and the ultrastructural and electrophysiological features of these “axon->glial” synapses have been investigated in slice preparations, generally by evoking potentials in local fiber bundles [1-4]. However, the afferent projections from neurons to OPCs providing this synaptic input have not been systematically mapped, and thus our understanding of the neuronal territories accessed by neuron->OPC synapses has been limited. Recent evidence has demonstrated that neuronal

activity robustly regulates OPC proliferation, oligodendrogenesis, and myelin sheath thickness in both juvenile and adult rodents [5-7] and also influences axon selection during developmental myelination in zebrafish [8,9]. These activity-regulated responses of oligodendroglial cells have been shown to confer adaptive changes in motor function [5], are necessary for some forms of motor learning [10,11] and contribute to cognitive behavioral functions such as attention and short-term memory [12]. Appreciation for this plasticity of myelin has stoked interest in the axon->glial synapse as a means by which OPCs could detect and integrate activity-dependent neuronal signals. Here, we employ a modified rabies virus-based monosynaptically-restricted trans-synaptic retrograde tracing strategy to elucidate a map of neuronal synaptic inputs to OPCs in the corpus callosum (CC), secondary motor cortex (MOs), and primary somatosensory cortex (SSp) *in vivo*. We find brain-wide, functionally-interconnected inputs to OPCs and that the degree of this connectivity is stable across brain region and is maintained despite whisker trimming-induced sensory deprivation in barrel cortex.

RESULTS

Development and validation of retrograde monosynaptic OPC tracing strategy

Owing to the lack of viral tools to achieve specific transgene expression in OPCs, we employed a transgenic strategy by crossing *Pdgfra::*CreER mice [13], which permit OPC-specific Cre recombinase expression, with a Cre-inducible RABVgp4/TVA mouse [14]. Offspring of this cross express rabies virus glycoprotein 4 and the avian TVA receptor specifically in OPCs upon tamoxifen administration (*Pdgfra*::CreER-(gp4-TVA)^{fl}). Subsequent stereotaxic injection of ASLV-A (EnvA)-pseudotyped gp4-deleted rabies virus encoding EGFP (SADΔG-EGFP(EnvA)) achieves cell-specific, Cre-dependent labeling of OPC starter cell populations (Figure 1A). Virus can then spread retrogradely across single synaptic connections to presynaptic input neurons, but further spread is prevented by lack of gp4 [15]. A caveat to this approach is that OPCs that differentiate to oligodendrocytes [16] between tamoxifen administration and virus injection would still be susceptible to infection; likewise, infected OPCs that undergo differentiation could skew

histological assessment of input to starter cell ratios. To mitigate these concerns, we followed a narrow injection time course (Figure 1A) beginning in adult (6-month old) mice, when rates of OPC differentiation are substantially lower than in juveniles [17].

3 days following a single dose of tamoxifen and 5 days following injection of SADΔG-EGFP(EnvA) into the genu of the corpus callosum inferior to the cingulum bundle, we observed substantial labeling of presynaptic neuronal inputs (Figure 1B). In control (gp4-TVA)^{fl} mice lacking the *Pdgfra*::CreER transgene, injection of tamoxifen and modified rabies virus achieved only minor, local background labeling expected to result from small fractions of EnvA negative viral particles (Figure 1C). Pdgfra+/Olig2+/EGFP+ starter cells were present in the injection site (Figure 1D), while other glial subtypes including Gfap+ white matter astrocytes as well as Iba1+ macrophages and microglia were EGFP negative, confirming the specificity of glial infection to the targeted OPC population (Figure S1A,B). Immunostaining for Cre expression at this timepoint confirmed previously-reported driver specificity to OPCs [13], with no expression of Cre in NeuN+ neurons in this context (Figure 1E). Thus, the starter cell population is limited to the oligodendroglial lineage, with no evidence of non-synaptic "leak" of virus into other cell populations. While viral infection did result in limited toxicity to infected OPCs as suggested by morphology, expression of the identifying markers, Pdgfra and Olig2, was retained (Figure S1C).

<u>OPCs in corpus callosum receive brain-wide synaptic input</u>

Quantification of input neurons revealed extensive neuronal territories that synapse onto starter OPCs in the corpus callosum (Figure 2A,B). Summing all inputs identified, viral input/starter ratios in this context are approximately 20 (slope of linear regression 20.47 ± 2.7 standard error, Figure 2C), with neuronal input cells clearly identifiable by morphology and EGFP expression (Figure 2D). Neuronal inputs to OPCs in the genu of the corpus callosum inferior to the cingulum bundle are concentrated in dorsal and ventral mPFC (defined here to include anterior

cingulate, pre- and infralimbic regions) and secondary motor cortex (MOs) (Figure 2E). Inputs from primary motor (MOp) and primary somatosensory (SSp) cortices are also present, along with substantial connectivity from the thalamus (TH, Figure 2E). These previously unidentified thalamic inputs are most consistently localized to ventroanterolateral (VAL), anteromedial (AM), and anterodorsal (AD) nuclei, consistent with thalamocortical projection neurons targeting motor and prefrontal cortical areas (Figure 5). The majority of inputs identified arise ipsilateral to the viral injection site; however, the relatively high contribution of inputs arising in the contralateral mPFC combined with high overall labeling densities in this region suggest that callosal OPCs are substantially innervated by contralateral intracortical mPFC projections (Figure 2F). By contrast, thalamic inputs are ipsilaterally restricted, further supporting the monosynaptic restriction of viral labeling (Figure 2F).

While GABAergic inputs to OPCs have been described [18,19], the majority of evidence for neuron-OPC synaptic connectivity in the corpus callosum arises from recordings of glutamatergic excitation either spontaneously or following callosal fiber stimulus [1,2]. Immunostaining for characteristic non-overlapping cortical inhibitory subpopulation markers accounting for the majority of total cortical inhibitory neurons [20] – parvalbumin (PV), vasoactive intestinal peptide (VIP), and somatostatin (SOM) – revealed PV+/GFP+ co-labeled inputs encompassing approximately 3% of inputs to OPCs in CC (Fig 2G). The majority of these PV+GFP+ inputs were present ipsilaterally in the overlying MOs/mPFC. SOM or VIP co-labeled GFP+ input neurons comprised 1% or less of total inputs to OPCs in the CC. The excitatory to inhibitory neuron ratio of inputs to callosal OPCs is ~20:1, with inhibitory neurons defined by PV, VIP or SOM-expression.

<u>OPCs in secondary motor cortex receive synaptic input from functionally associated cortical and thalamic neurons</u>

Examining the afferents to cortical OPCs in the secondary motor (premotor, MOs, M2) cortex, injection of SADΔG-EGFP(EnvA) into MOs of *Pdgfra*::CreER-(gp4-TVA)^{fl} mice (Figure 3B) again resulted in infection of Pdgfra+/EGFP+ starter OPCs. Labeled input neurons were strikingly predominant within functionally associated cortical territory defining the boundaries of MOs (Figure 3A,D). Input to starter cell ratios were not substantially different from those in CC-injected animals (slope of best-fit linear regression = 18.76 ± 4.4 standard error, Figure 3C). Beyond MOs, a smaller fraction of inputs arise from primary motor cortex (MOp), nearby medial prefrontal cortex (mPFC), and to a lesser extent, projections from SSp, and thalamocortical projection neurons (Figure 3D,E), illustrating brain-wide and circuit-specific inputs to premotor cortical OPCs. Immunostaining for markers of interneuron identity revealed PV+/GFP+ inputs averaging 6% of total input neurons to mPFC OPCs, while SOM+/GFP+ or VIP+/GFP+ costaining was present in approximately 1% or less of total inputs (Figure 3F). Input neurons to MOs OPCs are primarily ipsilateral, with a smaller proportion of afferent projections arising contralaterally than observed in OPCs within the CC (Figure 3G). Like CC OPCs, the excitatory to inhibitory ratio of inputs to premotor cortical OPCs is ~20:1, with inhibitory neurons defined by PV, VIP or SOM-expression.

<u>OPCs in primary somatosensory cortex receive synaptic input from ipsilateral local and functionally-associated thalamic neurons</u>

To assess whether the pattern of cortical OPC inputs arising from local cortical neurons and functionally-associated thalamic nuclei was specific to MOs, we injected SADΔG-EGFP(EnvA) into primary somatosensory cortex (SSp) of *Pdgfra*::CreER-(gp4-TVA)^{fl} mice (Fig 4B). As in MOs and CC, this resulted in primary infection of Pdgfra+/EGFP+ starter OPCs, and as in MOs, inputs were confined primarily to functionally related cortical territory (SSp) (Fig 4A). Input to starter cell ratios at this site did not differ significantly from injections in CC or MOs (slope of best-fit linear regression = 22.57 ± 3.8 standard error, Fig 4C). Examination of GFP+ input

neurons revealed inputs arising primarily from SSp across multiple cortical layers and thalamus (Fig 4D,E). In contrast to OPCs residing in CC, and to a lesser extent MOs, input neurons to OPCs in SSp are almost entirely ipsilaterally-restricted, and there is a small (<5%) contribution of input neurons from mPFC, MOs, or MOp. As in MOs, immunostaining for markers of interneuron identity revealed approximately 4% of GFP+ input neurons colabeled with PV, while SOM+ or VIP+ inputs comprised 1% or less of total GFP+ inputs (Fig 4F). Like CC and promotor cortex OPCs, the excitatory to inhibitory ratio of inputs to somatosensory cortical OPCs is ~20:1, with inhibitory neurons defined by PV, VIP or SOM-expression.

Thalamic input neurons to OPCs arise from functionally-related thalamic nuclei

For OPCs in all brain regions studied, a substantial fraction of synaptic inputs arise from thalamic neurons. To assess whether these thalamic inputs arise from functionally-related nuclei, we registered acquired image tiles to the Allen Institute reference adult mouse brain atlas [21] and localized identified GFP+ inputs (Figure 5). Thalamic projections providing synaptic input to OPCs located in the corpus callosum underlying primary and secondary motor cortex arise primarily from ventral anterior-lateral (VAL) and anteromedial (AM) nuclei, consistent with known projections to motor planning territories (Fig 5A), along with projections from the anterodorsal (AD) nucleus. Strikingly, thalamic inputs to MOs OPCs also arose primarily from VAL and AM nuclei (Fig 5B). This is largely distinct from thalamic projections to SSp OPCs, which arise primarily within ventral posterolateral (VPL) and ventral posteromedial (VPM) regions, consistent with known projections to somatosensory targets (Fig 5C). Together, this suggests that particularly in the case of cortical OPCs, these previously unidentified thalamocortical synaptic inputs arise from functionally-related thalamic nuclei.

Total synaptic connectivity to OPCs is consistent across brain regions despite reduced input neuron activity

To assess whether the degree of synaptic connections to OPCs varied across the injection sites assessed, we compared the average neuronal input ratios, assessed as the slope of the best-fit linear regression to total GFP+ inputs versus starter Pdgfra+/GFP+ OPCs. We found no significant difference in the synaptic input ratios between OPCs in the CC, MOs, or SSp (Fig 6A). To assess whether perturbations of synaptic input activity might modify the degree of synaptic connectivity, we performed daily whisker trimming of *Pdgfra*::CreER-(gp4-TVA)^{fl} mice for 11 days prior to tamoxifen injection (Fig 6B). Anticipating that input activity to the cortical barrel field would be reduced in whisker-trimmed animals, we then injected SADΔG-EGFP(EnvA) into barrel field of trimmed and matched untrimmed control animals. 5 days after viral injection, the animals were euthanized and total GFP+ input neurons and Pdgfra+/GFP+ starter OPCs were quantified. We found no significant difference in neuronal to starter input ratio between whisker-trimmed and untrimmed control animals as assessed by the slope of best-fit linear regression (Fig 6C,D). Moreover, we found no significant difference in the distribution of input neurons between trimmed and untrimmed animals, with primarily somatosensory cortical inputs and approximately 10% of inputs arising from thalamus (Fig 6E). Quantification of immunostaining for interneuron markers revealed PV+GFP+ inputs in equal proportion (3-4%) in trimmed and untrimmed groups (Fig 6F), indicating an unchanged excitatory to inhibitory (PV+ neuron) ratio of OPC inputs regardless of whisker trimming at this time point. Taken together, neither OPC location across white and gray matter territories, nor modification of input activity in barrel field by whisker trimming modified the quantity or pattern of neurons providing synaptic input to OPCs.

DISCUSSION

Substantial progress in characterizing the electrophysiological properties of neuron-OPC synapses has yet to clarify their potential role in modulating oligodendrocyte lineage dynamics and ultimately animal behavior. In particular, prior to this work little was known regarding the extent of neuronal input territories to OPCs beyond local neurons and fiber bundles accessible

in a slice preparation. Using a monosynaptically restricted trans-synaptic retrograde tracing system, we have now elucidated a map of neuronal input territories to OPCs in three distinct regions of the mouse brain. OPCs in these territories – selected due to previously reported changes in local oligodendrocyte lineage dynamics in response to neuronal activity – all receive brain-wide, circuit-specific synaptic input. Strikingly, the ratio of input neurons to starter OPCs is consistent across MOs, SSp, and CC, despite the much greater local axon density in CC and despite higher OPC turnover rates in CC than either cortical territory. This suggests that regulation of the number of neuron-OPC synapses may be intrinsic to the OPC rather than specified by local neurons or other microenvironmental factors in these brain regions.

While the estimated number of synaptic inputs appears consistent across mapped regions, the localization of these strikingly extensive inputs is distinct by location and support a pattern of functionally-associated brain-wide afferent connectivity to OPCs. For OPCs present in the CC genu inferior to the cingulum bundle, there is a relative bias of inputs from cortical regions involved in planning and execution of motor skills, and ~ 25% of these inputs arise contralateral to the targeted OPCs. While previous studies have demonstrated evoked synaptic inputs to these white matter OPCs by stimulation of callosal fibers, we now provide an unbiased assessment of the cortical projection neurons and interneurons responsible for these synapses, as well as previously unrecognized OPC inputs from thalamocortical projections. Notably, behavioral paradigms shown to alter oligodendrocyte lineage dynamics in mice, including motor learning tasks and social isolation, are thought to drive dynamic changes in neuronal activity in MOs and mPFC. We now demonstrate that the majority of synaptic inputs to these white matter OPCs arise from these very brain regions. These synaptic inputs are also largely excitatory, with immunostaining revealing a relatively small fraction of OPC inputs arising from local PV+ interneurons. Strikingly, this fraction is relatively consistent across cortical and white matter territories investigated here, which may result either from higher regional density of excitatory

projection axons or may indicate that OPCs actively regulate the number of interneuron inputs as a mechanism to maintain excitatory:inhibitory balance.

Our assessment of synaptic inputs to gray matter OPCs maps neuronal connectivity to this regionally and perhaps functionally distinct cell population. In contrast to callosal white matter OPCs, neuronal inputs to OPCs present in SSp or MOs primarily arise within ipsilateral local cortex, although a smaller fraction (mean approximately 7.5%) of inputs to OPCs in MOs arise contralaterally. Additionally, we identify functionally-associated thalamocortical projections providing previously unrecognized synaptic input to these OPCs. Taken together, the demonstrated map of input neurons to cortical OPCs suggests a mechanism by which OPCs could sense synchronized patterns of activity between thalamus and cortex. In turn, integration of this synaptic activity by individual OPCs might coordinate or regulate adaptive myelination of circuitry linking cortical and thalamic territories – a model that merits evaluation in future studies.

While the localization and laterality of neuronal input to OPCs varies depending on brain region, the total numerical extent of input connections – as measured by input:starter ratio – is remarkably consistent across territories. Given that the rate of OPC turnover in these regions has been shown to vary [22], it follows that the extent of synaptic input must be regulated by a newly-generated OPC to result in equivalent connectivity. OPCs in input-deprived somatosensory cortex following unilateral whisker trimming are less likely to survive in a critical temporal window following division, which subsequently results in diminished generation of mature oligodendrocytes [23]. Moreover, genetic ablation of AMPA receptors in OPCs reduces the survival of oligodendrocytes generated during development [24]. We now demonstrate that deprivation of input activity to barrel field OPCs by whisker trimming does not alter the synaptic input ratios of surviving cells, nor does it impact the distribution of neuronal inputs at the time point evaluated. This may suggest that the pool of OPCs giving rise to early oligodendrocytes in the above studies begin from the same level of synaptic connectivity. From this baseline, activity

deprivation-related deficits resulting in decreased survival may accumulate at later stages of cell differentiation. Alternatively, OPCs that fail to attain sufficient synaptic input in the critical window after division may fail to survive, resulting in deficient oligodendrogenesis despite apparently normal starter to input ratios. An important caveat to highlight is that, using this method we cannot delineate the connectivity of single cells, only the population total. This raises the possibility that a mixture of high and low-connectivity OPCs could exist, and newly-generated cells could tend to sort into one pool or the other under the control of local factors, however this possibility cannot be tested with existing methods and will remain a question for future work. This discovery of widespread, functionally-associated, and remarkably stable neuronal afferents to OPCs thus indicates a need to probe context-specific roles of neuron-OPC synaptic connectivity and ultimately to determine the function of these enigmatic structures.

Acknowledgements

We thank Brady Weissbourd for helpful discussion and Pamelyn Woo for assistance with animal colony maintenance. The authors gratefully acknowledge support from the California Institute for Regenerative Medicine (CIRM RN3-06510), National Institute of Neurological Disorders and Stroke (NINDS R01NS092597 and F31NS098554), NIH Director's Pioneer Award (DP1NS111132), SFARI Foundation, Maternal and Child Health Research Institute at Stanford

References

1 Ziskin, J., Nishiyama, A., Rubio, M., Fukaya, M. & Bergles, D. Vesicular release of glutamate from unmyelinated axons in white matter. *Nat Neurosci* **10**, 321-330, doi:10.1038/nn1854 (2007).

2 De Biase, L., Nishiyama, A. & Bergles, D. Excitability and synaptic communication within the oligodendrocyte lineage. *J Neurosci* **30**, 3600-3611, doi:10.1523/JNEUROSCI.6000-09.2010 (2010).

3 Kukley, M., Capetillo-Zarate, E. & Dietrich, D. Vesicular glutamate release from axons in white matter. *Nat Neurosci* **10**, 311-320, doi:10.1038/nn1850 (2007).

4 Lundgaard, I. *et al.* Neuregulin and BDNF induce a switch to NMDA receptor-dependent myelination by oligodendrocytes. *PLoS Biol* **11**, e1001743, doi:10.1371/journal.pbio.1001743 (2013).

5 Gibson, E. M. *et al.* Neuronal activity promotes oligodendrogenesis and adaptive myelination in the mammalian brain. *Science* **344**, 1252304, doi:10.1126/science.1252304 (2014).

6 Mitew, S. *et al.* Pharmacogenetic stimulation of neuronal activity increases myelination in an axon-specific manner. *Nat Commun* **9**, 306, doi:10.1038/s41467-017-02719-2 (2018).

7 Hughes, E. G., Orthmann-Murphy, J. L., Langseth, A. J. & Bergles, D. E. Myelin remodeling through experience-dependent oligodendrogenesis in the adult somatosensory cortex. *Nat Neurosci* **21**, 696-706, doi:10.1038/s41593-018-0121-5 (2018).

8 Mensch, S. *et al.* Synaptic vesicle release regulates myelin sheath number of individual oligodendrocytes in vivo. *Nat Neurosci* **18**, 628-630, doi:10.1038/nn.3991 (2015).

9 Hines, J. H., Ravanelli, A. M., Schwindt, R., Scott, E. K. & Appel, B. Neuronal activity biases axon selection for myelination in vivo. *Nat Neurosci* **18**, 683-689, doi:10.1038/nn.3992 (2015).

10 McKenzie, I. A. *et al.* Motor skill learning requires active central myelination. *Science* **346**, 318-322, doi:10.1126/science.1254960 (2014).

11 Xiao, L. *et al.* Rapid production of new oligodendrocytes is required in the earliest stages of motor-skill learning. *Nat Neurosci* **19**, 1210-1217, doi:10.1038/nn.4351 (2016).

12 Geraghty, A. C. *et al.* Loss of Adaptive Myelination Contributes to Methotrexate Chemotherapy-Related Cognitive Impairment. *Neuron*, doi:10.1016/j.neuron.2019.04.032 (2019).

13 Kang, S., Fukaya, M., Yang, J., Rothstein, J. & Bergles, D. NG2+ CNS glial progenitors remain committed to the oligodendrocyte lineage in postnatal life and following neurodegeneration. *Neuron* **68**, 668-681, doi:10.1016/j.neuron.2010.09.009 (2010).

14 Takatoh, J. *et al.* New modules are added to vibrissal premotor circuitry with the emergence of exploratory whisking. *Neuron* **77**, 346-360, doi:10.1016/j.neuron.2012.11.010 (2013).

15 Wickersham, I. R. *et al.* Monosynaptic restriction of transsynaptic tracing from single, genetically targeted neurons. *Neuron* **53**, 639-647, doi:10.1016/j.neuron.2007.01.033 (2007).

16 Ye, F. *et al.* HDAC1 and HDAC2 regulate oligodendrocyte differentiation by disrupting the beta-catenin-TCF interaction. *Nat Neurosci* **12**, 829-838, doi:10.1038/nn.2333 (2009).

17 Young, K. *et al.* Oligodendrocyte dynamics in the healthy adult CNS: evidence for myelin remodeling. *Neuron* **77**, 873-885, doi:10.1016/j.neuron.2013.01.006 (2013).

18 Kukley, M. *et al.* Glial cells are born with synapses. *FASEB J* **22**, 2957-2969, doi:10.1096/fj.07-090985 (2008).

19 Lin, S. C. & Bergles, D. E. Synaptic signaling between GABAergic interneurons and oligodendrocyte precursor cells in the hippocampus. *Nat Neurosci* **7**, 24-32, doi:10.1038/nn1162 (2004).

20 Pfeffer, C. K., Xue, M., He, M., Huang, Z. J. & Scanziani, M. Inhibition of inhibition in visual cortex: the logic of connections between molecularly distinct interneurons. *Nat Neurosci* **16**, 1068-1076, doi:10.1038/nn.3446 (2013).

21 Lein, E. S. *et al.* Genome-wide atlas of gene expression in the adult mouse brain. *Nature* **445**, 168-176, doi:10.1038/nature05453 (2007).

22 Rivers, L. *et al.* PDGFRA/NG2 glia generate myelinating oligodendrocytes and piriform projection neurons in adult mice. *Nat Neurosci* **11**, 1392-1401, doi:10.1038/nn.2220 (2008).

23 Hill, R., Patel, K., Goncalves, C., Grutzendler, J. & Nishiyama, A. Modulation of oligodendrocyte generation during a critical temporal window after NG2 cell division. *Nat Neurosci* **17**, 1518-1527, doi:10.1038/nn.3815 (2014).

24 Kougioumtzidou, E. *et al.* Signalling through AMPA receptors on oligodendrocyte precursors promotes myelination by enhancing oligodendrocyte survival. *Elife* **6**, doi:10.7554/eLife.28080 (2017).

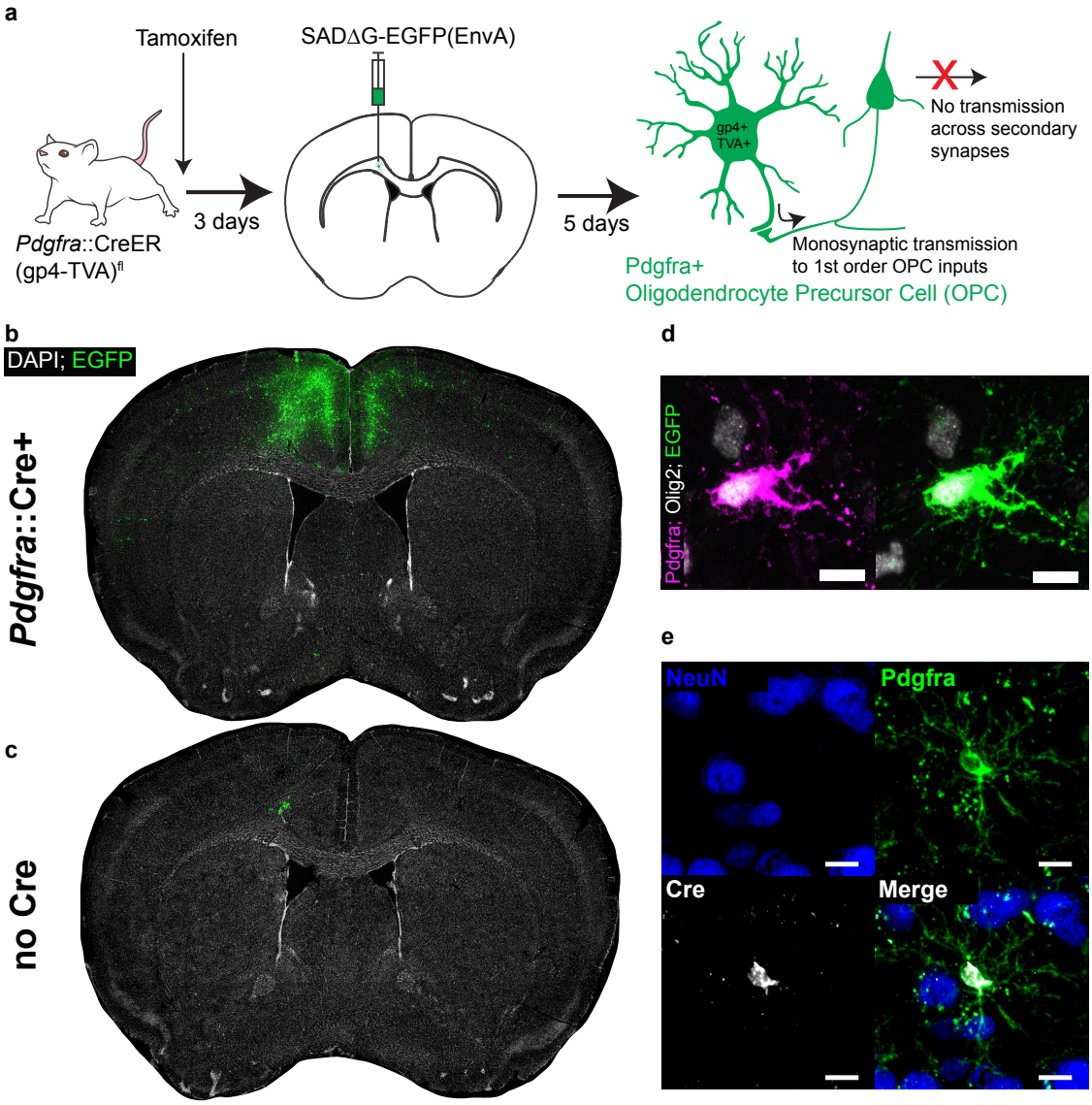

Figure 1. Monosynaptically-restricted rabies virus enables tracing of synaptic inputs to OPCs. (**a**) Outline of experimental strategy used to label inputs to Pdgfra+ OPCs. (**b**) Injection of SADΔG-EGFP(EnvA) into sub-cingular corpus callosum results in widespread labeling of EGFP+ input neurons (representative injection site image from n=10 animals. Green = EGFP, white = DAPI). (**c**) Injection of SADΔG-EGFP(EnvA) into animals lacking *Pdgfra*::CreER driver allele results in only minimal transduction, likely resulting from minimal quantities of EnvA- viral particles (representative image of n=4 animals. Green = EGFP, white = DAPI). (**d**) Pdgfra+/Olig2+ OPC starter cells (left) are transduced with SADΔG-EGFP(EnvA) (right, same cell. Magenta = Pdgfra, white = Olig2, green = EGFP). (**e**) Immunostaining confirms Cre recombinase expression in Pdgfra+ OPCs (green) but not NeuN+ neurons (blue). Scale bars in (d,e) represent 10 microns.

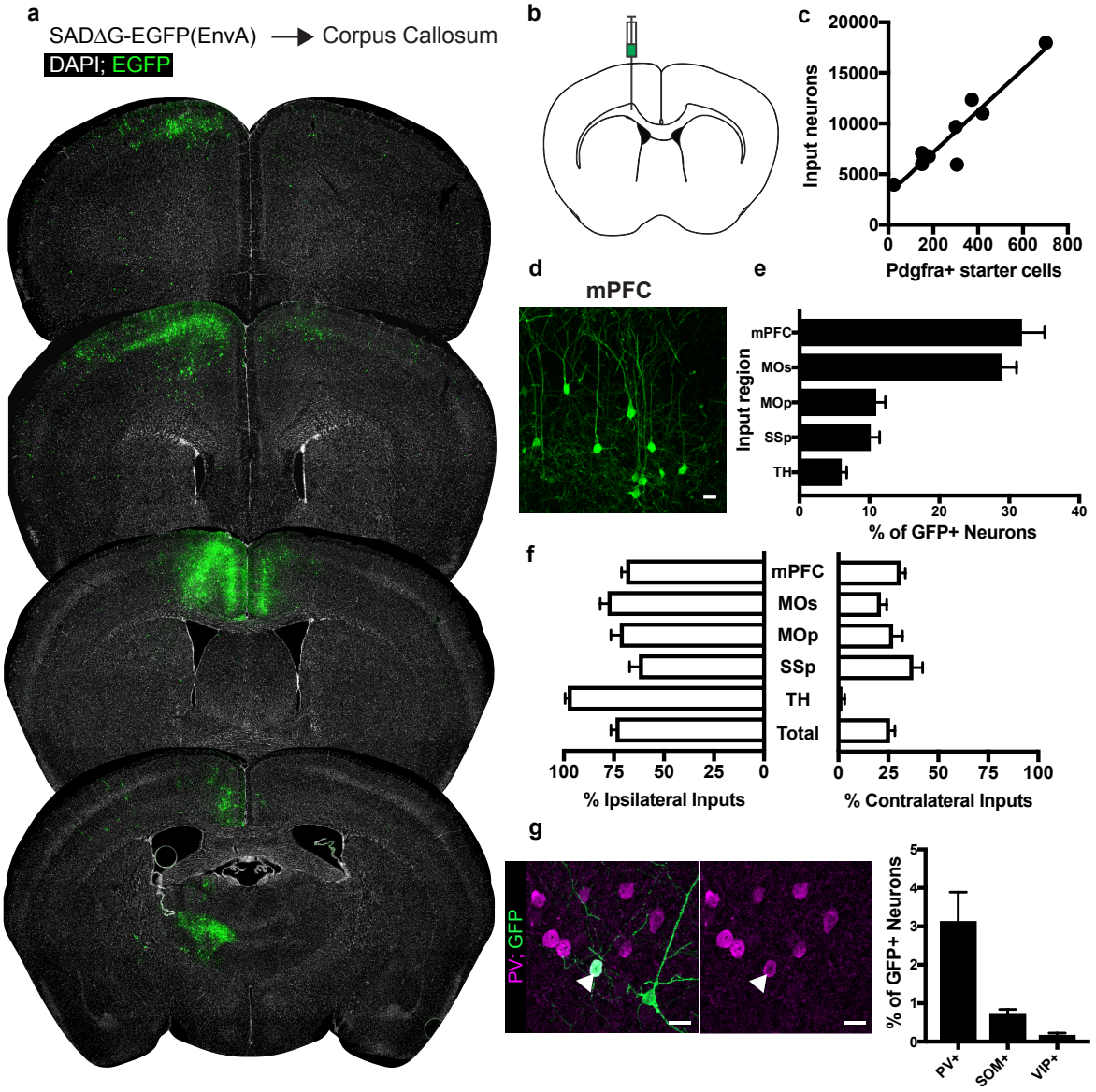

Figure 2. Neuronal inputs to callosal OPCs arise from functionally interconnected cortical and thalamic areas. (**a**) Representative sections of neuronal input labeling to OPCs following stereotaxic injection of SADΔG-EGFP(EnvA) to corpus callosum underlying the secondary motor area. Green = EGFP, white = DAPI. (**b**) Schematic of injection site. (**c**) Linear regression fit of neuronal input/Pdgfra+ OPC starter cells. Each point represents one animal, R^2 = 0.8909, slope = 20.47 ± 2.7 standard error. (**d**) Representative confocal micrograph of EGFP+ (green) input neurons in medial prefrontal (mPFC) cortex. (**e**) Inputs to callosal OPCs largely arise from frontal association cortices but also include primary motor and somatosensory areas and thalamic nuclei. Each bar represents mean input percentage, error bars indicate SEM, n=10 total. mPFC = medial prefrontal cortex (anterior cingulate, prelimbic, infralimbic regions), MOs = secondary motor area, MOp = primary motor area, SSp = primary somatosensory area, TH = thalamus (including all thalamic nuclei). (**f**) Percent of input neurons ipsilateral or contralateral to the OPC starter cells. Bars indicate mean, error bars indicate SEM, n=10 animals. (**g**) Representative image of parvalbumin+ (PV+, magenta) GFP+ (green) input neuron and quantification of percentage of input neurons that co-label with immunofluorescence makers for

PV, somatostatin (SOM), or vasoactive intestinal peptide (VIP). Bars represent mean, error bars indicate SEM, n=6 total. Scale bars in (d,g) represent 20 microns.

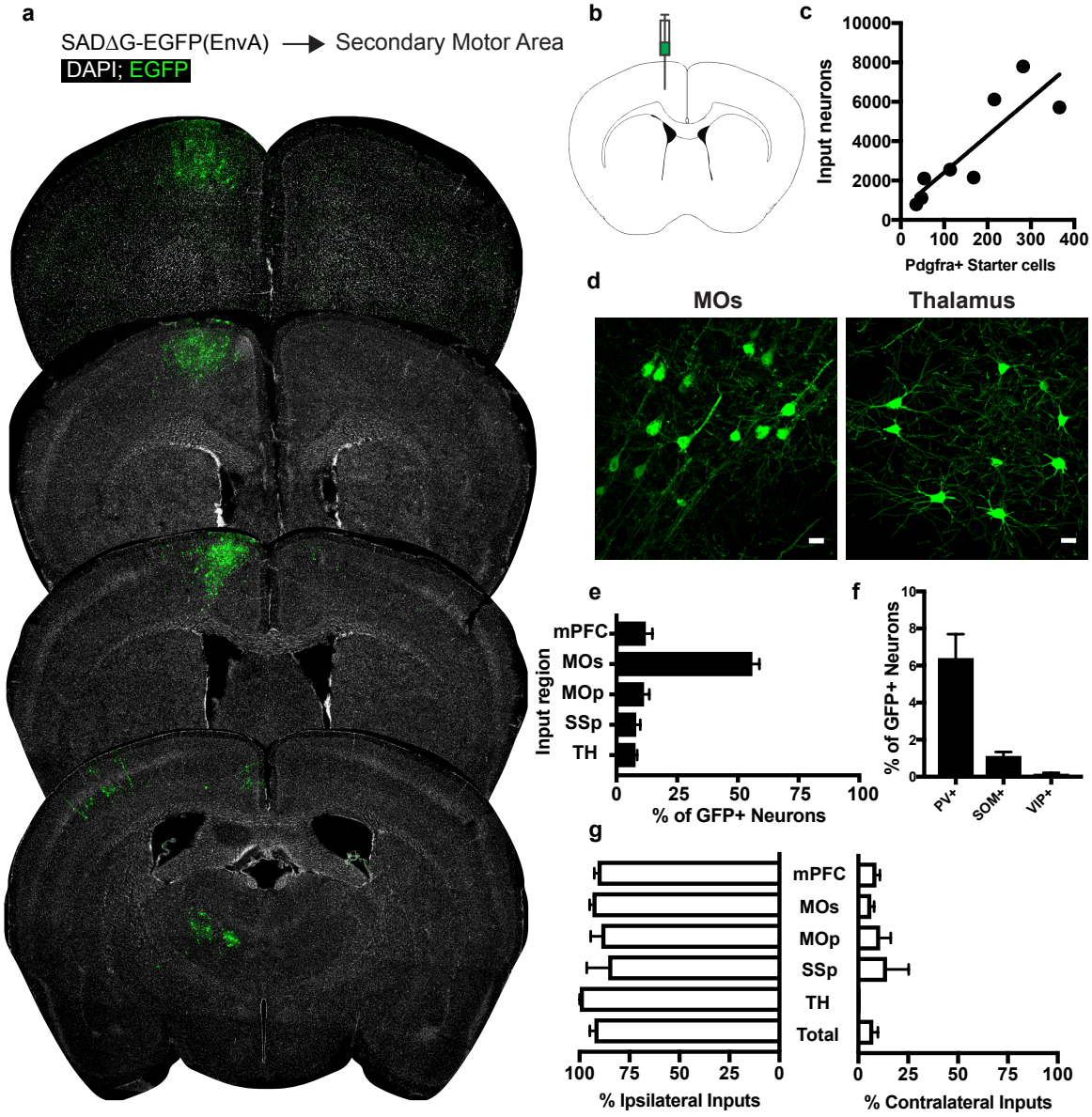

Figure 3. Circuit-specific cortical and thalamic neuronal inputs to OPCs in secondary motor area (MOs) (**a**) Representative sections of neuronal input labeling to OPCs following stereotaxic injection of SADΔG-EGFP(EnvA) to MOs. Green = EGFP, white = DAPI. (**b**) Schematic of injection site. (**c**) Linear regression fit of neuronal input/Pdgfra+ starter cells. Each point represents one animal, R^2 = 0.7486, slope = 18.76 ± 4.4 standard error). (**d**) Representative confocal micrographs of EGFP+ (green) input neurons in secondary motor cortex (MOs) and thalamus. (**e**) Inputs to grey matter OPCs found in MOs are chiefly located within MOs, n = 8 animals total. mPFC = medial prefrontal cortex (anterior cingulate, prelimbic, infralimbic regions), MOs = secondary motor area, MOp = primary motor area, SSp = primary somatosensory area, TH = thalamus (including all thalamic nuclei). (**f**) Percentage of input neurons that co-label with immunofluorescence makers for parvalbumin (PV), somatostatin (SOM), or vasoactive intestinal peptide (VIP), n=5. (**g**) Percent of input neurons ipsilateral or

contralateral to OPC starter cells. Bars indicate mean, error bars indicate SEM, each point represents an individual animal (n=8). Scale bars in (d) represent 20 microns.

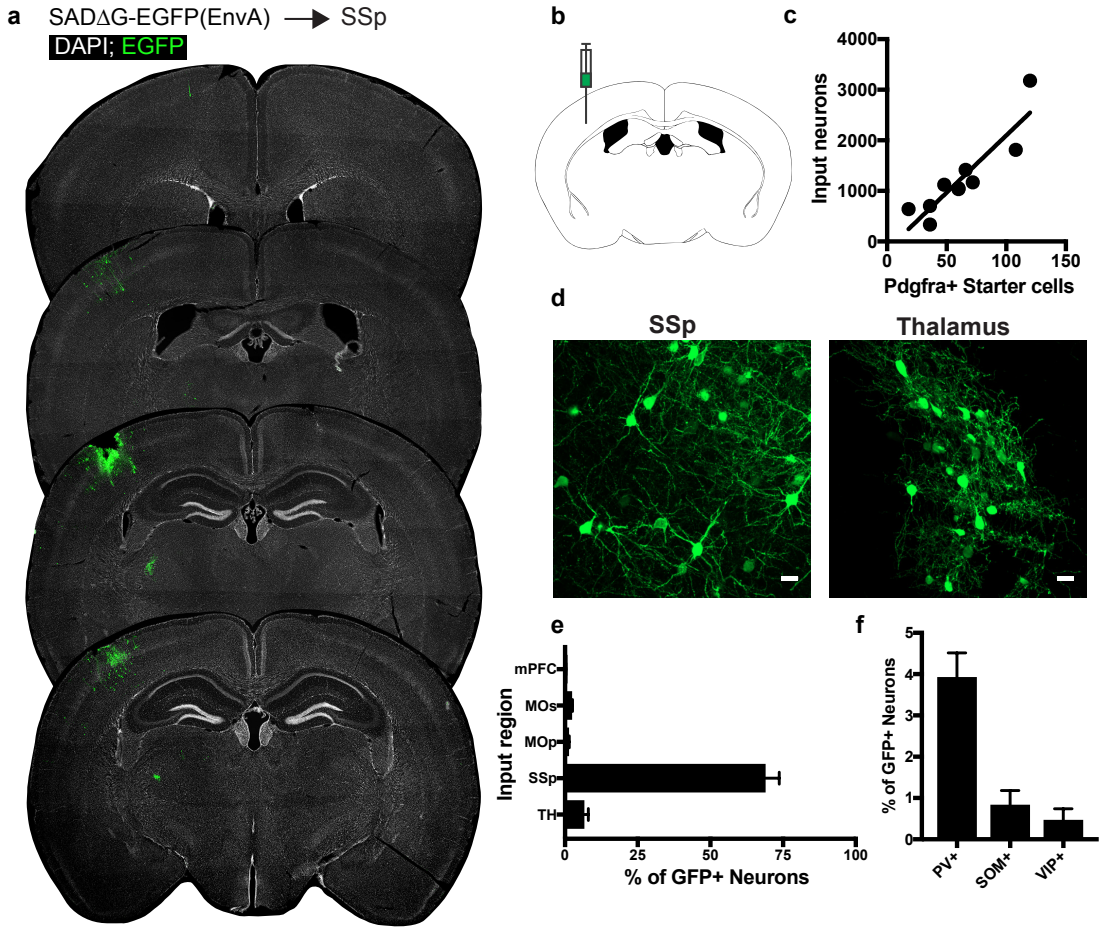

Figure 4. Circuit-specific cortical and thalamic neuronal neuronal inputs to SSp (**a**) Representative sections of neuronal input labeling to OPCs following stereotaxic injection of SADΔG-EGFP(EnvA) to SSp. Green = EGFP, white = DAPI. (**b**) Schematic of injection site. (**c**) Linear regression fit of neuronal input/Pdgfra+ starter cells. Each point represents one animal, R^2 = 0.8145, slope = 22.57 ± 3.8 standard error). (**d**) Representative confocal micrographs of EGFP+ (green) input neurons in primary somatosensory cortex (SSp) and thalamus. (**e**) Inputs to grey matter OPCs found in SSp are chiefly located within SSp. n = 9 animals total. mPFC = medial prefrontal cortex (anterior cingulate, prelimbic, infralimbic regions), MOs = secondary motor area, MOp = primary motor area, SSp = primary somatosensory area, TH = thalamus (including all thalamic nuclei). (**f**) Percentage of input neurons that co-label with immunofluorescence makers for parvalbumin (PV), somatostatin (SOM), or vasoactive intestinal peptide (VIP), n = 5 animals. Bars indicate mean, error bars indicate SEM. Scale bars in (d) represent 20 microns.

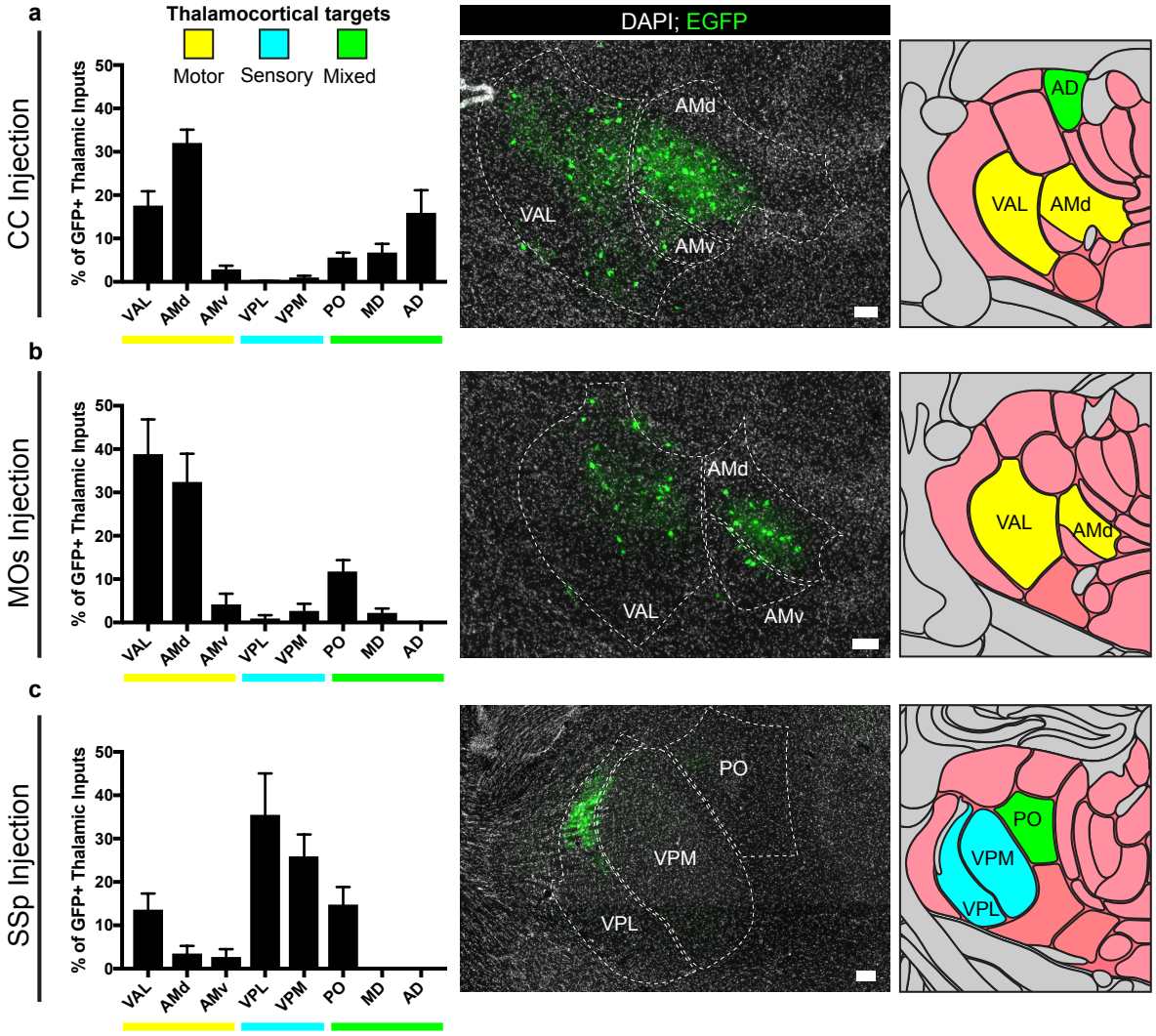

Figure 5. Thalamic inputs to OPCs arise from functionally-related nuclei. Tiled immunofluorescence images of GFP+ input neurons were registered to the Allen Brain Atlas to determine the thalamic nuclei from which the inputs arise. Nuclei are color-coded here according to the primary function of their cortical projection targets – motor (yellow), sensory (blue), or mixed (green). (**a**) Thalamic inputs to OPCs in the CC underlying primary and secondary motor cortices arise primarily from ventral anterior-lateral (VAL) and anteriomedial (AM) nuclei. (**b**) Thalamic inputs to OPCs in MOs arise primarily from VAL and AM nuclei. (**c**) Thalamic inputs to SSp arise primarily from ventral posterolateral (VPL) and ventral posteromedial (VPM) nuclei. All bars indicate mean, error bars indicate SEM. Scale bars represent 100 microns. N = 10 mice (CC), 8 mice (MOs), and 6 mice (SSp) respectively. Thalamic nuclei defined as presented in the Allen Brain Atlas and abbreviated as follows: VAL = ventral anterior-lateral, AMd = anteromedial dorsal part, AMv = anteromedial ventral part, VPL= ventral posterolateral, VPM = ventral posteromedial, PO = posterior complex, MD = mediodorsal, AD = anterodorsal.

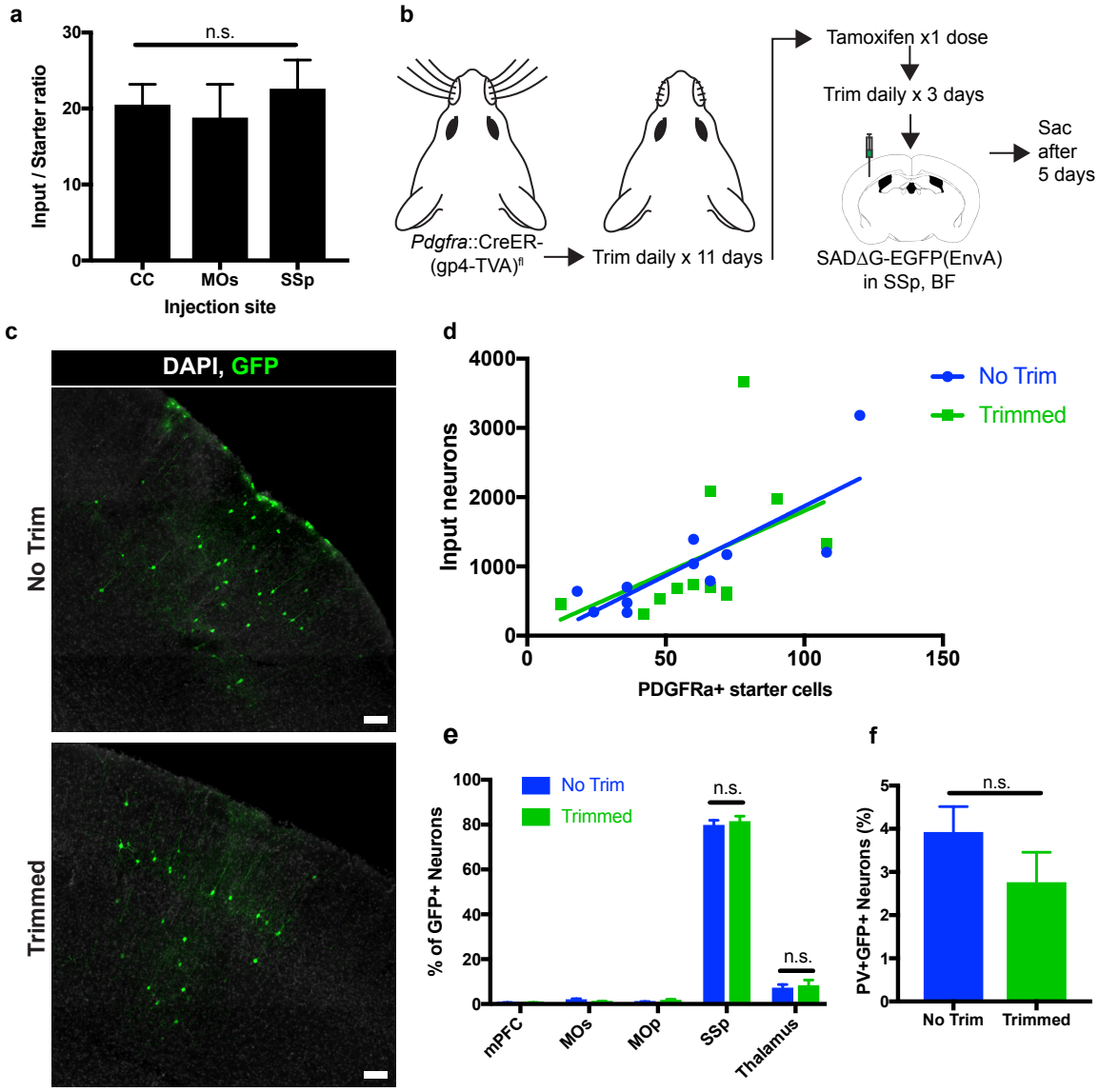

Figure 6. Neuronal input to OPC starter ratios are consistent across brain region and despite whisker trimming-induced activity deprivation. (**a**) Neuronal input to OPC starter ratios, as measured by the slope of the best-fit linear regression of GFP+ input neurons against Pdgfra+/GFP+ OPC starter cells. Bars indicate mean, error bars indicate standard error of linear regression. (**b**) Outline of whisker trimming deprivation expriment and subsequent viral injection into barrel field of somatosensory cortex (SSp,BF). (**c**) Representative images of GFP+ input neurons in SSp, BF of non-trimmed and trimmed animals, white = DAPI, green = GFP. (**d**) Scatter plot of GFP+ input neurons against Pdgfra+/GFP+ starter OPCs and best-fit linear regression to assess average input to starter cell ratio in whisker-trimmed (Trimmed) and control (No Trim) groups. Each point represents an independent animal, n = 13 (Trimmed), n = 11 (No Trim). (**e**) Distribution of GFP+ neuronal inputs to OPCs in Trimmed and No Trim groups as a percentage of total inputs. n = 13 (Trimmed), n = 11 (No Trim). (**f**) Proportion of total GFP+ input neurons immunostaining for parvalbumin (PV) in Trimmed and No Trim groups, n=5 each. Bars indicate mean, error bars indicate SEM. Scale bars in (c) represent 100 microns. Statistical testing performed by Tukey's multiple comparisons test, n.s. indicates p>0.05.

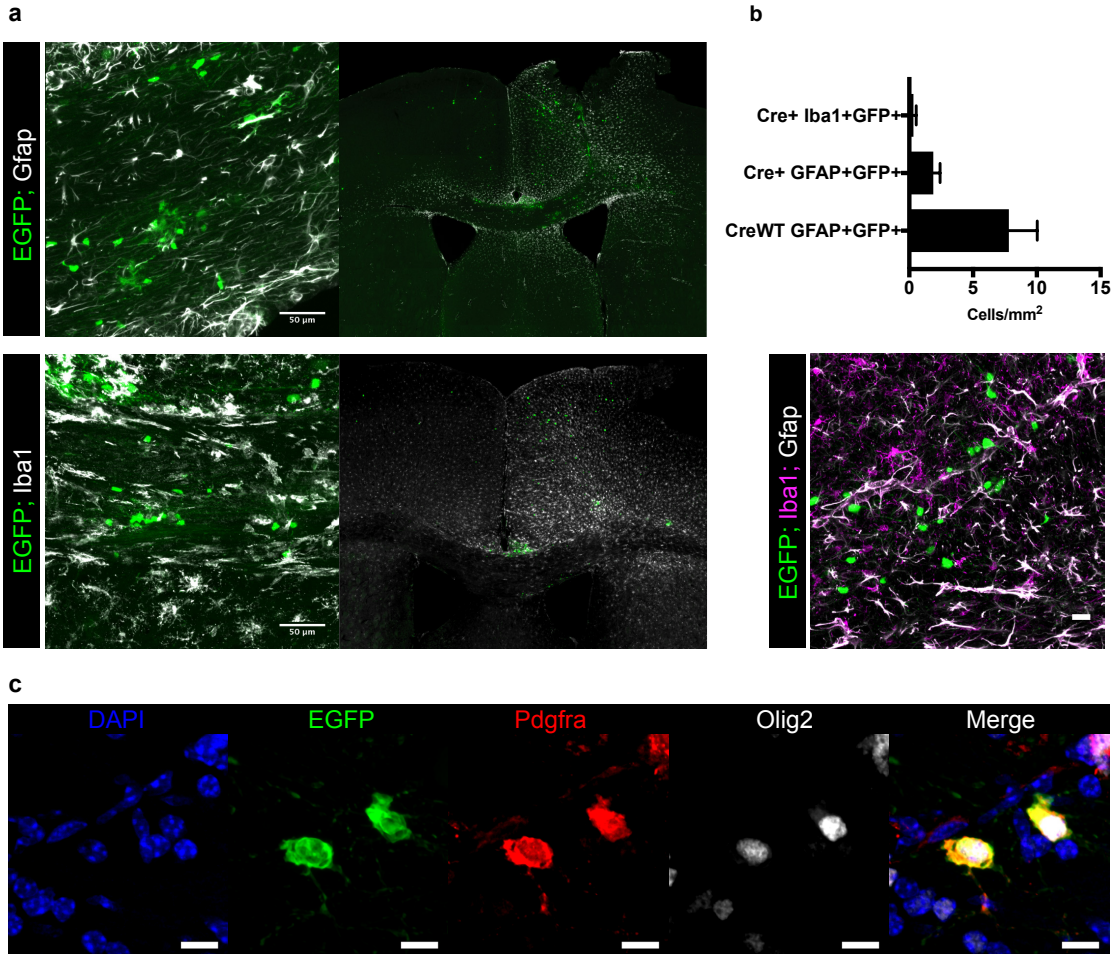

Figure S1. Related to Figure 1. SADΔG-EGFP(EnvA) does not substantially infect other glial subtypes. **(a)** Immunofluorescence staining for the white matter and reactive astrocyte marker Gfap (white; top panels) and the macrophage marker Iba1 (white; bottom panels) does not identify substantial evidence of EGFP+ (green) astroglial/microglial cells despite evidence of reactive gliosis in the injection site. **(b)** Quantification of colocalization studies represented in (a) demonstrates minimal overlap concentrated to the injection site that is not increased in Cre+ animals compared with minimal expected background labeling in Cre WT controls. In the representative merged image from a quantified region, green = EGFP; magenta = Iba1; white = Gfap. **(c)** Example of EGFP+Pdgfra+Olig2+ starter cells with disrupted morphology. Blue = DAPI, green = EGFP; red = Pdgfra; white = Olig2. Bars indicate the mean, n=6 animals (Cre WT) or 9 animals (Cre+) respectively; error bars represent SEM. Scale bars in (a) are 50 microns, in (b) are 20 microns, and in (c) are 10 microns.

Methods

Animal breeding

All animal studies were approved by the Stanford Administrative Panel on Laboratory Animal Care (APLAC). Animals were housed on a 12hr light cycle according to institutional guidelines. Mice expressing CreER under the control of *Pdgfra* promoter/enhancer regions (*Pdgfra*::Cre/ERT) were purchased from The Jackson Laboratory (stock number 018280) and have been previously described[13]. Mice expressing a recombinant rabies G glycoprotein gene (*RABV*gp4) along with the gene encoding avian leucosis and sarcoma virus subgroup A

receptor (*TVA*) preceded by a *loxP*-flanked STOP fragment and inserted into the *GT(ROSA)26Sor* locus (R26(gp4-TVA)$^{fl/fl}$) have been previously described[14] and were purchased from The Jackson Laboratory (stock number 024708). Hemizygous *Pdgfra*::Cre/ERT mice were then crossed with homozygous R26(gp4-TVA)$^{fl/fl}$ mice to generate animals used in subsequent experiments. Genotyping was performed by PCR according to supplier protocols.

Viral tracing

EGFP-expressing G-deleted rabies virus pseudotyped with EnvA (SADΔG-EGFP(EnvA))[15] was prepared at and obtained from the Salk Institute Gene Transfer, Targeting, and Therapeutics Facility vector core (GT3). Virus used in these studies originated in two lots with reported titers of $7.92x10^7$ and $1.94x10^9$ TU/mL. 3 days prior to stereotaxic injections, Cre/ERT-mediated recombination was induced by a single IP injection of 100mg/kg of tamoxifen (Sigma) solubilized in corn oil. Stereotaxic delivery of virus occurred under isofluorane anesthesia in BSL2+ conditions. 300nL of SADΔG-EGFP(EnvA) was delivered to the corpus callosum (coordinates AP +1mm, ML – 1mm, DV -1.2mm) or the overlying secondary motor area (coordinates AP + 1mm, ML – 0.8mm, DV -0.5mm) or primary somatosensory cortex (coordinates AP -1mm, ML -3mm, DV -0.7mm) over 5 minutes (Stoelting stereotaxic injector). Animals were monitored for general health, and no adverse symptoms of viral administration were observed. 5 days following viral injection, animals were deeply anesthetized with tribromoethanol and transcardially perfused with PBS followed by 4% PFA, then brains were removed and post-fixed overnight in 4% PFA. Brains were then transferred to 30% sucrose, and after sinking serial 40 micrometer floating coronal sections were prepared on a freezing-stage microtome for subsequent immunolabeling and imaging.

Whisker trimming

Pdgfra::CreERT; R26(gp4-TVA)^{fl} mice generated as described above were trimmed of whiskers bilaterally to the level of the skin using electric clippers daily beginning at P25. At P37, tamoxifen was injected as described above, and whisker trimming continued daily until P40, when SADΔG-EGFP(EnvA) was injected as described above. Animals were then sac'd and perfused at P45 as described above.

Immunofluorescence and confocal microscopy

Antibodies and dilutions used for immunofluorescence staining were as follows: polyclonal goat anti-mouse Pdgfra (R&D Systems, AF1062, 1:500), monoclonal rabbit anti-mouse Olig2 (Abcam EPR2673, 1:500), polyclonal chicken anti-GFP (Abcam, ab13970, 1:1000), polyclonal rabbit anti-parvalbumin (Abcam, ab11427, 1:250), monoclonal rat anti-somatostatin (Millipore, MAB354, 1:200), polyclonal rabbit anti-VIP (Immunostar 20077, 1:500), polyclonal rabbit anti-Iba1 (Wako, 1:500), and mouse anti-Cre recombinase (Millipore, MAB3120, clone 2D8, 1:1000). Tissues collected at serial intervals of 1 in every 6 sections were blocked and permeabilized with 3% normal donkey serum and 0.3% Triton X-100 in Tris-Buffered Saline (3%NDS/TBST) for 30 minutes at room temperature, followed by incubation with antibodies at the indicated dilution factors in 1%NDS/TBST for 18 hours at 4 degrees C. For mouse anti-Cre recombinase staining, NDS block was followed by treatment with mouse-on-mouse staining reagent (Vector Laboratories, BMK-2202) prior to incubation with primary antibody. Following a series of washes, secondary AlexaFluor-tagged antibodies raised in donkey (Jackson Immunoresearch) in 1%NDS/TBST were incubated for 4 hours at room temperature, and following a series of washes, sections were counterstained with DAPI (1ug/mL) and mounted on slides with ProlongGold media (ThermoFisher Scientific). Tile scanning images were acquired at 10X magnification on a Zeiss AxioObserver upright fluorescence microscope with automated stage and tile-scanning capability (Microbrightfield). For identification of atlas regions for labeling quantification, acquired images were manually registered to the closest available section from the Allen Brain Mouse Reference Atlas[21] (ImageJ) using DAPI fluorescence of the section outline and major neuroanatomical structures to guide fitting. Analysis participants were blinded

to injection conditions, and independent adjustment of atlas registration maps did not substantially impact counting results. Cell counting was performed by two independent reviewers on every 6th 40 micrometer tissue section throughout the brain, and total cell count estimates were derived by multiplying the number of counted cells by 6. Multichannel immunofluorescence microscopy to identify starter cell populations, neuronal identity, and other high-resolution imaging was conducted by acquiring Z-stacks through the target region with a Zeiss LSM710 confocal microscope.

Statistics and reproducibility

Stereotaxic injections were repeated in 3 independent cohorts (litters) of animals for each injection location, and both male and female mice were used. Sample sizes were established based upon similar studies in the literature and were not pre-determined. Cell counters were blinded to injection location, and counts were performed independently by two reviewers. All statistical tests were performed using Graphpad Prism software and details of individual tests are described in figure legends.

Data availability statement

The data that support the findings of this study are available from the corresponding author upon reasonable request.